(Received 10 March 2026, Accepted 8 April 2026, Scheduled 13 May 2026)

Unified Analytical and Numerical Evaluation of Axial Magnetic Force in Coaxial Air-Core Coils

Ali Jebelli[1,*], Nafiseh Lotfi[2], Arezoo Mahabadi[3], and Mustapha C. E. Yagoub[4]

[1] College of Business, Engineering and Technology, Kentucky State University, Kentucky, USA
[2] Department of Engineering and Design, Robotic Century, Kentucky, USA
[3] Department of Engineering and Design, Robotic Century, Alberta, Canada
[4] School of Electrical Engineering and Computer Science, University of Ottawa, Ontario, Canada

ABSTRACT: Accurate prediction of magnetic interaction forces is important for electromagnetic actuators, inductive coupling systems, and calibration devices. This paper presents a unified analytical and numerical framework for evaluating the axial magnetic force between two finite-dimensional, perfectly coaxial, air-core cylindrical coils under steady currents. The model assumes uniform purely azimuthal current density and neglects radial and axial current components, winding-pitch effects, magnetic materials, misalignment, and transient phenomena. Starting from the Biot-Savart law and Lorentz force formulation, the coil-coil interaction integral is derived and reduced using cylindrical symmetry, leaving only the axial resultant force. Three complementary methods are developed in MATLAB: a semi-analytical elliptic-integral formulation, a direct trapezoidal numerical-integration method, and a filament-based mutual-inductance method. The methods are computationally benchmarked for representative thin-wall, moderate finite-radius, mixed-radius, and large finite-radius coil geometries. The results show consistent force predictions, with relative half-spread values below approximately 4% for the cases considered. Discretization sensitivity and error-source analysis are included to clarify numerical accuracy and convergence. The proposed framework provides a transparent benchmark for axial force evaluation in idealized coaxial air-core coil systems.

1. INTRODUCTION

Magnetic fields and the forces generated by current-carrying coils play a central role in many electromagnetic and electromechanical systems. In configurations involving coaxial coils, the axial magnetic interaction force directly affects actuation capability, mechanical stability, positioning accuracy, coupling efficiency, and overall system performance. Accurate prediction of this force is therefore important in electromagnetic actuators, inductive coupling systems, wireless power transfer devices, force-calibration platforms, superconducting coil systems, and laboratory benchmark configurations [1–6].

For steady-current air-core systems, the magnetic field can be obtained from the Biot-Savart law, while the mechanical force acting on a current distribution follows from the Lorentz force formulation. Combining these two laws leads to a volume-volume interaction integral between the source and receiving coils [4]. Although the governing physical laws are well established, their direct application to coils with finite radial thickness and finite axial length produces multidimensional integrals that are not always convenient for repeated engineering calculations. As a result, practical force evaluation often relies either on simplified analytical models, such as circular-loop, thin-wall, or disk-coil approximations, or on full numerical field simulations, which can be accurate but computationally expensive and less transparent for parametric analysis [5, 6].

Classical analytical and semi-analytical methods based on mutual inductance, elliptic integrals, and Maxwell-type formulations have been widely used for calculating magnetic fields, inductances, and forces in circular loops, thin-wall coils, and coaxial solenoids [1–3, 7–13]. These methods are attractive because they provide compact expressions and high computational efficiency under idealized geometric assumptions. Numerical methods based on direct integration of the Biot-Savart and Lorentz force laws provide a more general route within the assumed geometry, but their accuracy and computational cost depend strongly on discretization strategy, quadrature resolution, and the treatment of near-singular interaction regions.

Recent studies have continued to develop faster and more general approaches for coil modeling and electromagnetic computation. Fast analytic-numerical algorithms have been proposed for calculating self- and mutual inductances of air coils, while efficient semi-analytical formulations have also been extended to radial and axial magnetic forces between non-coaxial coils with rectangular cross-sections [14, 15]. Biot-Savart-based field-calculation methods have been reported for coreless circular coils with rectangular cross-sections and arbitrary turn numbers [16]. Reduced filament-based approaches have also been developed to calculate finite-cross-section coil self-fields, self-forces, and self-inductances with a lower computational burden than fully resolved volume models [19]. In parallel, machine-learning-assisted and reduced-order electromagnetic modeling has emerged as a promising direction for accelerating repeated field evaluation, surrogate modeling, and optimization [17, 18, 21]. Recent sensitivity-based coil-design studies further show that coil misalignment can introduce lateral-

* Corresponding author: Ali Jebelli (ali.jebelli@kysu.edu).

force components and significantly affect magnetic-force behavior, highlighting the limitations of strictly coaxial formulations when applied to imperfect real systems [20].

Despite these advances, analytical, direct numerical, and discretized filament-based approaches are often presented separately, with limited comparison under identical assumptions. This makes it difficult to determine how different methods behave for the same coil geometry, current distribution, axial separation, and numerical resolution. In particular, there remains a need for a unified formulation in which semi-analytical elliptic-integral methods, direct numerical integration, and filament-based mutual-inductance methods can be derived from the same governing electromagnetic principles and compared systematically in terms of accuracy, convergence behavior, and computational efficiency.

To address this need, this paper presents a unified analytical and numerical framework for evaluating the axial magnetic force between two finite-dimensional, perfectly coaxial, air-core cylindrical coils under steady current excitation. The coils are modeled using a continuous and uniform purely azimuthal current density. Therefore, the radial and axial current-density components are neglected, namely $J_r = 0$ and $J_z = 0$, while $J_\phi \neq 0$. This approximation is suitable for idealized, tightly wound cylindrical coils in which the dominant current direction is circumferential. Effects associated with helical winding pitch, local conductor routing, discrete turn spacing, current redistribution, magnetic materials, eddy currents, transient excitation, and coil misalignment are outside the scope of the present formulation.

Starting from the Biot-Savart law and the Lorentz force formulation, the general coil-coil interaction integral is derived and reduced using cylindrical symmetry. Under the assumption of perfect coaxial alignment, the net radial and azimuthal force components vanish after integration over the full angular domain, leaving only the axial resultant force. From this common theoretical foundation, three complementary computational approaches were developed and implemented in MATLAB:

(i) a semi-analytical method based on elliptic-integral reduction,

(ii) a direct multidimensional numerical-integration method using trapezoidal discretization, and

(iii) a filament-based method derived from Maxwell's mutual-inductance formulation.

The main contribution of this work is not the introduction of a new electromagnetic law, but the development of a consistent, transparent, and reproducible computational framework that unifies three commonly used modeling strategies for axial force evaluation in coaxial air-core coils. By deriving all three methods from the same physical formulation and applying them to identical validation geometries, the study enables direct comparison of their numerical agreement, discretization sensitivity, convergence behavior, and computational performance. The validation presented in this work is therefore interpreted as computational cross-validation within the stated assumptions, rather than experimental validation of practical wound-coil assemblies.

The proposed framework is useful for benchmark generation, preliminary electromagnetic actuator design, verification of numerical solvers, parametric force analysis, and educational treatment of coil-coil magnetic interaction problems. For systems involving magnetic cores, nonlinear permeability, significant misalignment, complex conductor routing, or transient excitation, the present methods should be regarded as an idealized benchmark or preliminary design tools rather than replacements for full three-dimensional electromagnetic simulation.

The remainder of this paper is organized as follows. Section 2 presents the theoretical formulation of the axial magnetic force between finite coaxial coils. Section 3 describes the three computational methods and their implementation. Section 4 presents the validation results, convergence behavior, and comparative analysis. Section 5 discusses practical applicability, limitations, and error sources. Section 6 summarizes the main conclusions.

2. THEORETICAL FORMULATION

2.1. Geometry and Current-Density Assumptions

Two finite-dimensional cylindrical air-core coils are considered. The coils are perfectly coaxial and share a common symmetry axis, chosen as the z-axis. Coil 1 has inner radius $R_{1,\text{in}}$, outer radius $R_{1,\text{out}}$, axial length L_1, number of turns N_1, and current I_1. Coil 2 is defined analogously by $R_{2,\text{in}}$, $R_{2,\text{out}}$, L_2, N_2, and I_2. The center-to-center axial separation between the two coils is denoted by H.

A point inside coil i is described in cylindrical coordinates as

$$\mathbf{r}_i = R_i \cos\phi_i \hat{\mathbf{x}} + R_i \sin\phi_i \hat{\mathbf{y}} + z_i \hat{\mathbf{z}}, \quad i = 1, 2.$$

The separation vector between two differential current elements is

$$\mathbf{R} = \mathbf{r}_2 - \mathbf{r}_1,$$

with magnitude

$$|\mathbf{R}| = \left[R_1^2 + R_2^2 + (z_2 - z_1)^2 - 2R_1R_2\cos(\phi_2 - \phi_1)\right]^{1/2}.$$

In the present formulation, each coil is modeled as a continuous current distribution with uniform purely azimuthal current density,

$$\mathbf{J}_i = J_{\phi,i}\hat{\boldsymbol{\phi}}_i, \quad i = 1, 2, \tag{1}$$

where

$$J_{\phi,i} = \frac{N_i I_i}{A_{c,i}},$$

and $A_{c,i}$ is the effective winding cross-sectional area of coil i. For a finite-volume rectangular winding region,

$$A_{c,i} = (R_{i,\text{out}} - R_{i,\text{in}})\, L_i.$$

Thus,

$$J_{r,i} = 0, \;\; J_{z,i} = 0, \;\; J_{\phi,i} \neq 0.$$

This means that radial and axial current-density components are neglected. The model therefore does not include local helical winding pitch, conductor end effects, turn-to-turn current redistribution, or any axial current component associated with

practical winding geometry. Thin-wall or zero-radial-thickness cases are interpreted as limiting filament or surface-current cases rather than finite-volume current-density cases.

2.2. Magnetic Field from the Biot-Savart Law

The magnetic flux density generated by the steady current distribution in Coil 1 is given by the Biot-Savart law,

$$\mathbf{B}_1(\mathbf{r}_2) = \frac{\mu_0}{4\pi}\int_{V_1}\frac{\mathbf{J}_1(\mathbf{r}_1)\times(\mathbf{r}_2-\mathbf{r}_1)}{|\mathbf{r}_2-\mathbf{r}_1|^3}dV_1, \tag{2}$$

where μ_0 is the permeability of free space. In cylindrical coordinates, the differential volume element is

$$dV_i = R_i dR_i d\phi_i dz_i.$$

2.3. Lorentz Force and Axial Force Kernel

The magnetic force acting on Coil 2 due to the magnetic field generated by Coil 1 is obtained from the Lorentz force law,

$$\mathbf{F}^{(2\leftarrow1)} = \int_{V_2}\mathbf{J}_2(\mathbf{r}_2)\times\mathbf{B}_1(\mathbf{r}_2)dV_2. \tag{3}$$

Substituting Eq. (2) into Eq. (3) gives the coupled volume-volume interaction integral

$$\mathbf{F}^{(2\leftarrow1)} = \frac{\mu_0}{4\pi}\int_{V_2}\int_{V_1}\frac{\mathbf{J}_2(\mathbf{r}_2)\times[\mathbf{J}_1(\mathbf{r}_1)\times(\mathbf{r}_2-\mathbf{r}_1)]}{|\mathbf{r}_2-\mathbf{r}_1|^3}dV_1dV_2. \tag{4}$$

Using the vector triple-product identity,

$$\mathbf{a}\times(\mathbf{b}\times\mathbf{c}) = \mathbf{b}(\mathbf{a}\cdot\mathbf{c}) - \mathbf{c}(\mathbf{a}\cdot\mathbf{b}),$$

with

$$\mathbf{a}=\mathbf{J}_2,\quad \mathbf{b}=\mathbf{J}_1,\quad \mathbf{c}=\mathbf{r}_2-\mathbf{r}_1,$$

one obtains

$$\mathbf{J}_2\times[\mathbf{J}_1\times(\mathbf{r}_2-\mathbf{r}_1)] = \mathbf{J}_1\left[\mathbf{J}_2\cdot(\mathbf{r}_2-\mathbf{r}_1)\right] - (\mathbf{r}_2-\mathbf{r}_1)(\mathbf{J}_2\cdot\mathbf{J}_1).$$

Because $\mathbf{J}_1$ is purely azimuthal, it has no z-component. Therefore, the first term does not contribute to the axial force. The axial component is determined by the second term. Since

$$\mathbf{J}_2\cdot\mathbf{J}_1 = J_{\phi,1}J_{\phi,2}\hat{\boldsymbol{\phi}}_2\cdot\hat{\boldsymbol{\phi}}_1 = J_{\phi,1}J_{\phi,2}\cos(\phi_2-\phi_1),$$

the axial component becomes

$$\{\mathbf{J}_2\times[\mathbf{J}_1\times(\mathbf{r}_2-\mathbf{r}_1)]\}\cdot\hat{\mathbf{z}} = -J_{\phi,1}J_{\phi,2}(z_2-z_1)\cos(\phi_2-\phi_1).$$

Thus, the signed axial force on Coil 2 due to Coil 1 is

$$F_z^{(2\leftarrow1)} = -\frac{\mu_0}{4\pi}\int_{V_2}\int_{V_1}\frac{J_{\phi,1}J_{\phi,2}(z_2-z_1)\cos(\phi_2-\phi_1)}{|\mathbf{r}_2-\mathbf{r}_1|^3}dV_1dV_2. \tag{5}$$

The sign of $F_z^{(2\leftarrow1)}$ depends on the chosen positive z-direction. For two coils carrying currents in the same azimuthal direction and separated along positive z, the force is attractive; therefore, the force on the upper coil acts in the negative z-direction. In the results section, the force magnitude $|F_z|$ is reported when only the interaction strength is compared.

2.4. Cancellation of Radial and Azimuthal Force Components

For the idealized geometry considered here, the net radial and azimuthal force components vanish by cylindrical symmetry. The two-coil system is invariant under arbitrary rotation about the common z-axis. A nonzero resultant radial or azimuthal force would define a preferred transverse direction, which would contradict this rotational invariance.

Equivalently, in the integral formulation, the transverse force components contain sine and cosine factors of the absolute azimuthal coordinate. For every differential current element at an angular position ϕ, there exists a corresponding element at $\phi+\pi$ that produces an equal and opposite transverse contribution. Integration over the complete angular domain therefore cancels the radial and azimuthal components. The axial component is invariant under rotation and remains nonzero.

Because the interaction depends only on the relative azimuthal angle

$$\psi = \phi_2 - \phi_1,$$

the two angular integrations can be reduced as

$$\int_0^{2\pi}\int_0^{2\pi} g(\phi_2-\phi_1)d\phi_1 d\phi_2 = 2\pi\int_0^{2\pi} g(\psi)d\psi.$$

Since the axial-force kernel is even in ψ, this may also be written as

$$2\pi\int_0^{2\pi} g(\psi)d\psi = 4\pi\int_0^{\pi} g(\psi)d\psi.$$

Using the cylindrical volume elements, Eq. (5) can therefore be reduced to the five-dimensional form

$$F_z^{(2\leftarrow1)} = -\mu_0\int_{z_2}\int_{z_1}\int_{R_2}\int_{R_1} J_{\phi,1}J_{\phi,2}R_1R_2(z_2-z_1)\left[\int_0^{\pi}\frac{\cos\psi}{D^{3/2}}d\psi\right]dR_1dR_2dz_1dz_2, \tag{6}$$

where

$$D = R_1^2 + R_2^2 + (z_2-z_1)^2 - 2R_1R_2\cos\psi. \tag{7}$$

Equation (6) is the main Lorentz-force interaction expression used as the basis for the direct numerical integration method.

2.5. Elliptic-Integral Form for Coaxial Circular Loops

For two coaxial circular current loops of respective radii R_1 and R_2, separated by an axial distance

$$s = z_2 - z_1,$$

the angular interaction can be expressed using complete elliptic integrals. The elliptic modulus is

$$k^2 = \frac{4R_1R_2}{(R_1+R_2)^2+s^2},\quad 0\le k\le 1. \tag{8}$$

The complete elliptic integrals of the first and second kind are defined as

$$K(k) = \int_0^{\pi/2}\frac{d\theta}{\sqrt{1-k^2\sin^2\theta}}, \tag{9}$$

and

$$E(k) = \int_0^{\pi/2} \sqrt{1 - k^2 \sin^2\theta}\, d\theta. \tag{10}$$

The mutual inductance between two coaxial circular loops is given by Maxwell's classical expression,

$$M(R_1, R_2, s) = \mu_0 \sqrt{R_1 R_2} \left[\left(\frac{2}{k} - k \right) K(k) - \frac{2}{k} E(k) \right]. \tag{11}$$

The axial force between the two circular loops can then be obtained from the derivative of the mutual inductance with respect to axial separation:

$$F_{z,\mathrm{l}}^{(2\leftarrow 1)} = I_1 I_2 \frac{\partial M(R_1, R_2, s)}{\partial s}. \tag{12}$$

An explicit expression for this derivative is

$$\frac{\partial M}{\partial s} = -\frac{\mu_0 s k}{4\sqrt{R_1 R_2}(1 - k^2)} \left[(2 - k^2)E(k) - 2(1 - k^2)K(k) \right]. \tag{13}$$

Equivalently, the same loop-loop axial force can be written in angular-integral form as

$$F_{z,\mathrm{l}}^{(2\leftarrow 1)} = -\mu_0 I_1 I_2 R_1 R_2 s \int_0^{\pi} \frac{\cos\psi}{\left[R_1^2 + R_2^2 + s^2 - 2R_1 R_2 \cos\psi\right]^{3/2}} d\psi. \tag{14}$$

Equations (11)–(14) provide the analytical basis for the semi-analytical and filament-based formulations used later in the paper. Only the complete elliptic integrals $K(k)$ and $E(k)$ are required for the Maxwell loop mutual-inductance formulation used here.

2.6. Finite-Coil Force from Loop Interaction

For finite coils with nonzero radial thickness and axial length, the total force can be obtained by integrating the loop-loop interaction over the radial and axial dimensions of both coils. The differential current carried by a small radial-axial element of coil i is

$$dI_i = J_{\phi,i} dR_i dz_i. \tag{15}$$

Therefore, the finite-coil axial force can be written as

$$F_z^{(2\leftarrow 1)} = \int_{z_{2,\min}}^{z_{2,\max}} \int_{z_{1,\min}}^{z_{1,\max}} \int_{R_{2,\mathrm{in}}}^{R_{2,\mathrm{out}}} \int_{R_{1,\mathrm{in}}}^{R_{1,\mathrm{out}}} J_{\phi,1} J_{\phi,2} \frac{\partial M(R_1, R_2, z_2 - z_1)}{\partial s} dR_1 dR_2 dz_1 dz_2. \tag{16}$$

This expression also defines the loop-interaction kernel used in the semi-analytical formulation:

$$f(R_1, R_2, s, k) = J_{\phi,1} J_{\phi,2} \frac{\partial M(R_1, R_2, s)}{\partial s}. \tag{17}$$

Thus, f represents the differential force contribution between two circular current filaments located at radii R_1 and R_2 and separated by axial distance s.

For thin-wall or zero-radial-thickness configurations, Eq. (16) is interpreted in the surface-current or filament limit. In that case, the radial integration is replaced by evaluation at the specified coil radius, and the current is assigned according to the corresponding loop or surface-current representation.

2.7. Basis for the Computational Methods

The theoretical formulation above provides a common basis for the three computational approaches developed in this study.

First, the semi-analytical method evaluates the finite-coil force using the elliptic-integral mutual-inductance expression in Eq. (11) and its axial derivative in Eq. (13).

Second, the direct numerical integration method evaluates the Lorentz-force integral in Eq. (6) using numerical quadrature over the radial, axial, and relative azimuthal coordinates.

Third, the filament-based method discretizes each finite coil into a finite array of circular current loops and sums the pairwise loop forces computed from Eq. (12) or Eq. (13).

Because all three approaches originate from the same Biot-Savart and Lorentz-force formulation, they can be compared under identical assumptions regarding geometry, current density, and axial separation.

3. COMPUTATIONAL METHODS

The axial-force formulation derived in Section 2 leads to a multidimensional interaction integral for finite coaxial coils. Although the governing expression follows directly from the Biot-Savart law and the Lorentz force formulation, its direct evaluation can be computationally demanding when both coils have finite radial thickness and finite axial length. Therefore, three complementary computational methods were developed and implemented in MATLAB:

1. a semi-analytical elliptic-integral method,
2. a direct multidimensional numerical-integration method, and
3. a filament-based mutual-inductance method.

All three methods are derived from the same theoretical formulation and use the same geometric and current-density assumptions. The methods differ only in how the coil-coil interaction kernel is evaluated or discretized. This common basis allows direct comparison of accuracy, convergence behavior, and computational cost.

3.1. Semi-Analytical Elliptic-Integral Method

The semi-analytical method evaluates the finite-coil force by reducing the angular interaction between two coaxial circular current loops to elliptic-integral form. This method is computationally efficient because the azimuthal dependence is represented analytically through the mutual-inductance function, while the remaining finite radial and axial dimensions are handled by numerical quadrature.

For two circular current loops of radii R_1 and R_2, separated by an axial distance

$$s = z_2 - z_1,$$

the loop-loop interaction is calculated using the Maxwell mutual-inductance expression $M(R_1, R_2, s)$ defined in Eq. (11). The axial force between two differential current loops is obtained from

$$dF_z = dI_1 dI_2 \frac{\partial M(R_1, R_2, s)}{\partial s}, \tag{18}$$

where $\partial M/\partial s$ is given in Eq. (13). For finite-volume coils, the differential current carried by a small radial-axial element is

$$dI_i = J_{\phi,i} dR_i dz_i. \tag{19}$$

Thus, the finite-coil axial force is evaluated as

$$F_z = \int_{z_{2,\min}}^{z_{2,\max}} \int_{z_{1,\min}}^{z_{1,\max}} \int_{R_{2,\text{in}}}^{R_{2,\text{out}}} \int_{R_{1,\text{in}}}^{R_{1,\text{out}}} J_{\phi,1} J_{\phi,2} \frac{\partial M(R_1, R_2, z_2 - z_1)}{\partial s} dR_1 dR_2 dz_1 dz_2. \tag{20}$$

Using quadrature weights, Eq. (20) is approximated by

$$F_z \approx \sum_a \sum_b \sum_c \sum_d w_{R_1,a} w_{R_2,b} w_{z_1,c} w_{z_2,d} J_{\phi,1} J_{\phi,2} \frac{\partial M(R_{1,a}, R_{2,b}, s)}{\partial s}\Big|_{s=z_{2,d}-z_{1,c}}. \tag{21}$$

The loop-loop force kernel used in this method is therefore

$$f(R_1, R_2, s, k) = J_{\phi,1} J_{\phi,2} \frac{\partial M(R_1, R_2, s)}{\partial s}, \tag{22}$$

which is consistent with the definition introduced in Eq. (17).

In MATLAB, the complete elliptic integrals are evaluated using standard numerical elliptic-integral routines. Since MATLAB uses the elliptic parameter $m = k^2$, the implementation evaluates the elliptic functions using m rather than k directly. This distinction is maintained throughout the numerical implementation to avoid the ambiguity between the elliptic modulus and elliptic parameter.

For thin-wall cases, where $R_{\text{in}} = R_{\text{out}}$, the finite-volume current-density expression is not used directly because the radial cross-sectional area becomes zero. Instead, the coil is treated as a surface-current or filament-limit case. In this limit, the radial integration is replaced by evaluation at the specified coil radius, and the current is assigned according to the corresponding surface-current or circular-loop representation.

The semi-analytical method is used as a fast benchmark solution for the idealized coaxial air-core configurations considered in this study.

3.2. Direct Numerical Integration Method

The direct numerical integration method evaluates the Lorentz-force interaction integral without elliptic-integral reduction. This approach preserves the full integral structure of the force formulation and provides a transparent numerical reference for the other two methods.

Using the cylindrical symmetry reduction derived in Section 2, the signed axial force can be written as

$$F_z = -\mu_0 \int_{z_2} \int_{z_1} \int_{R_2} \int_{R_1} J_{\phi,1} J_{\phi,2} R_1 R_2 (z_2 - z_1) \left[\int_0^{\pi} \frac{\cos\psi}{D^{3/2}} d\psi \right] dR_1 dR_2 dz_1 dz_2, \tag{23}$$

where

$$D = R_1^2 + R_2^2 + (z_2 - z_1)^2 - 2R_1 R_2 \cos\psi, \tag{24}$$

and

$$\psi = \phi_2 - \phi_1$$

is the relative azimuthal angle between two current elements.

The radial, axial, and angular coordinates are discretized as, respectively, $R_{1,a}$, $R_{2,b}$, $z_{1,c}$, $z_{2,d}$, ψ_e.

Using the composite trapezoidal rule, Eq. (23) is approximated by

$$F_z \approx -\mu_0 J_{\phi,1} J_{\phi,2} \sum_a \sum_b \sum_c \sum_d \sum_e w_{R_1,a} w_{R_2,b} w_{z_1,c} w_{z_2,d} w_{\psi,e} \frac{R_{1,a} R_{2,b} (z_{2,d} - z_{1,c}) \cos\psi_e}{D_{abcde}^{3/2}}, \tag{25}$$

where

$$D_{abcde} = R_{1,a}^2 + R_{2,b}^2 + (z_{2,d} - z_{1,c})^2 - 2R_{1,a} R_{2,b} \cos\psi_e. \tag{26}$$

For a uniformly spaced coordinate x, the trapezoidal weights are defined as

$$w_x = \begin{cases} \Delta x/2, & \text{at the first and last grid points,} \\ \Delta x, & \text{at interior grid points.} \end{cases} \tag{27}$$

This weighting is applied independently in the R_1, R_2, z_1, z_2, and ψ directions. The factors $R_1 R_2$ in Eq. (25) account for the cylindrical volume elements

$$dV_i = R_i dR_i d\phi_i dz_i.$$

The direct numerical integration method is implemented using vectorized MATLAB operations. Vectorization reduces nested-loop overhead and allows the interaction kernel to be evaluated over multidimensional arrays. For configurations with small axial separation, the grid resolution is refined to reduce near-singular quadrature error. Cases involving overlapping current volumes are excluded from the present formulation.

Although this method is computationally more expensive than the semi-analytical method, it is useful because it evaluates the Lorentz-force formulation directly and does not rely on mutual-inductance reduction.

3.3. Filament-Based Mutual-Inductance Method

The filament-based method approximates each finite coil as an array of circular current filaments distributed across its radial and axial cross-section. The total axial force is then obtained by summing all pairwise loop-loop force contributions.

For coil i, the winding cross-section is divided into $N_{R,i}$ radial divisions and $N_{z,i}$ axial divisions. A filament located at radial position $R_{i,a}$ and axial position $z_{i,c}$ carries the differential current

$$\Delta I_{i,ac} = J_{\phi,i}\Delta R_i \Delta z_i. \tag{28}$$

When trapezoidal or nonuniform quadrature is used, the product $\Delta R_i \Delta z_i$ is replaced by the corresponding quadrature weights,

$$\Delta I_{i,ac} = J_{\phi,i} w_{R_i,a} w_{z_i,c}. \tag{29}$$

For thin-wall or surface-current cases, the radial integration is removed, and the filament current is assigned from the appropriate loop-current or nsurface-current representation.

The axial force contribution between filament (a, c) in Coil 1 and filament (b, d) in Coil 2 is

$$\Delta F_{z,acbd} = \Delta I_{1,ac}\Delta I_{2,bd} \frac{\partial M(R_{1,a}, R_{2,b}, s)}{\partial s}|_{s=z_{2,d}-z_{1,c}}. \tag{30}$$

The total axial force is therefore

$$F_z = \sum_{a=1}^{N_{R,1}} \sum_{c=1}^{N_{z,1}} \sum_{b=1}^{N_{R,2}} \sum_{d=1}^{N_{z,2}} \Delta F_{z,acbd}. \tag{31}$$

The same elliptic-integral derivative in Eq. (13) is used to evaluate each filament-pair interaction. Thus, the filament-based method is physically consistent with the semi-analytical method, but the finite coil geometry is represented by discrete loop elements rather than continuous radial and axial integration.

The filament-based method offers a practical compromise between computational speed and modeling flexibility. It is generally faster than direct multidimensional integration and more flexible than a single analytical loop expression. However, its accuracy depends on the number and placement of filaments, especially for coils with large radial thickness or strong field gradients.

3.4. Implementation Procedure

For each validation case, the computational procedure is as follows.

First, the coil geometry, current, number of turns, and axial separation are specified. For finite-volume coils, the effective current density is calculated from

$$J_{\phi,i} = \frac{N_i I_i}{(R_{i,\text{out}} - R_{i,\text{in}})\, L_i}. \tag{32}$$

For thin-wall or filament-limit cases, the corresponding surface-current or loop-current representation is used instead.

Second, the axial coordinate ranges of the two coils are defined relative to their centers. If Coil 1 is centered at $z = 0$ and Coil 2 centered at $z = H$, then

$$z_1 \in \left[-\frac{L_1}{2}, \frac{L_1}{2}\right], \tag{33}$$

and

$$z_2 \in \left[H - \frac{L_2}{2}, H + \frac{L_2}{2}\right]. \tag{34}$$

Third, the axial force is evaluated using the three methods described above. For each method, the signed force F_z is calculated first. When only the interaction strength is compared, the magnitude $|F_z|$ is reported.

Fourth, convergence is assessed by refining the discretization parameters. For the direct numerical integration method, the radial, axial, and angular grid densities are increased until the change in $|F_z|$ between two successive refinements falls below a prescribed tolerance. For the filament-based method, the number of filaments in the radial and axial directions is increased until the computed force becomes insensitive to further refinement.

3.5. Error Metrics and Convergence Assessment

To compare the three computational methods quantitatively, two error measures are used. When one method or one grid level is selected as a reference solution, the relative error of method m is defined as

$$\delta_m = 100\frac{|F_m - F_{\text{ref}}|}{|F_{\text{ref}}|}. \tag{35}$$

For convergence plots, the non-percentage relative force error is written as

$$\varepsilon = \frac{|F_\Delta - F_{\text{ref}}|}{|F_{\text{ref}}|}, \tag{36}$$

where F_Δ is the force obtained at normalized grid step size Δ. Unless otherwise stated, F_{ref} is taken as the finest-grid numerical solution.

When the purpose is to measure the spread among the three methods without assigning a single reference solution, the relative half-spread is defined as

$$\delta_{\text{half}} = 100\frac{F_{\max} - F_{\min}}{2\bar{F}}, \tag{37}$$

where

$$\begin{aligned} F_{\max} &= \max\left(|F_1|, |F_2|, |F_3|\right), \\ F_{\min} &= \min\left(|F_1|, |F_2|, |F_3|\right), \end{aligned}$$

and

$$\bar{F} = \frac{|F_1| + |F_2| + |F_3|}{3}.$$

Here, F_1, F_2, and F_3 denote the force values obtained from the semi-analytical, direct numerical-integration, and filament-based methods, respectively.

TABLE 1. Comparative summary of the computational methods.

Method	Main computational kernel	Main advantage	Main limitation
Semi-analytical elliptic-integral method	$\partial M/\partial s$ using $K(k)$ and $E(k)$	Fast evaluation and useful benchmark solution	Restricted to idealized coaxial air-core geometry
Direct numerical integration method	Discretized Lorentz-force integral	Most direct representation of the governing force integral	Highest computational cost
Filament-based mutual-inductance method	Pairwise loop-loop mutual-inductance derivative	Good balance between speed and flexibility	Accuracy depends on filament density

For the composite trapezoidal rule, the expected convergence rate for a sufficiently smooth integrand is

$$\varepsilon = O(\Delta^2), \tag{38}$$

where Δ is the characteristic normalized grid spacing. In practice, the convergence rate may be affected by near-singular behavior at small separations, finite grid resolution, and the distributed nature of the current density. Therefore, convergence is evaluated numerically for the validation cases rather than assumed solely from the formal order of the quadrature rule.

The main numerical and modeling error sources considered in this study are quadrature error, filament discretization error, near-singular kernel behavior, elliptic-integral evaluation sensitivity, and geometric idealization error. Quadrature error arises in the direct numerical-integration and semi-analytical finite-coil integrations. Filament discretization error arises because a continuous current distribution is approximated by a finite number of circular loops. Near-singular kernel behavior becomes important when interacting current elements are very close. Elliptic-integral evaluation sensitivity may occur when k approaches unity. Geometric idealization error results from the assumptions of perfectly coaxial alignment, air-core medium, and uniform purely azimuthal current density.

3.6. Comparative Characteristics of the Methods

The three methods have complementary advantages and limitations. The semi-analytical elliptic-integral method is the fastest method and is well suited for rapid parametric analysis under the idealized coaxial assumptions. The direct numerical integration method is slower but provides the most direct evaluation of the Lorentz-force integral. The filament-based method provides an intermediate approach, combining reasonable computational efficiency with a clear physical interpretation in terms of interacting circular current loops. Table 1 summarizes the main computational kernel, principal advantage, and primary limitation of each method, highlighting the complementary roles of the semi-analytical elliptic-integral method, direct numerical integration method, and filament-based mutual-inductance method.

Because the three methods originate from the same Biot-Savart and Lorentz-force formulation, agreement among them provides an internal consistency check. However, such an agreement should be interpreted as computational cross-validation rather than experimental validation. Experimental force measurements or independent finite-element benchmarks are required to assess deviations caused by winding pitch, conductor spacing, manufacturing tolerances, material effects, and measurement uncertainty.

4. RESULTS AND VALIDATION

To evaluate the numerical consistency, convergence behavior, and computational performance of the proposed unified framework, the three computational approaches developed in Section 3 were applied to representative coaxial air-core coil configurations. The methods compared in this section are the semi-analytical elliptic-integral method, the direct numerical integration method, and the filament-based mutual-inductance method.

The purpose of this section is to provide computational validation and internal cross-comparison under identical modeling assumptions. The validation presented here should therefore be interpreted as analytical and numerical benchmark validation, not as experimental validation. Experimental force measurements are outside the scope of the present work and are identified as a future extension in Section 5.

All simulations were performed in MATLAB using double-precision arithmetic. The same geometric parameters, current values, number of turns, and axial separation distances were used for the three computational methods in each validation case. Unless otherwise stated, the reported force values correspond to the magnitude of the axial force, $|F_z|$. The sign convention follows the formulation in Section 2, where the force direction depends on the selected positive z-axis and relative current directions.

4.1. Validation Configurations

Four representative coil configurations were selected to test the proposed framework over a range of idealized and finite-volume geometries. These cases were chosen to examine the behavior of the methods for thin-wall, moderate finite-radius, mixed-radius, and large finite-radius coil systems.

The validation cases are:

1. thin-wall configuration, representing the limiting case of circular loop-like coils with negligible radial thickness;
2. moderate finite-radius configuration, representing two identical coils with finite radial width;
3. mixed-radius configuration, representing two coils with different radial dimensions;

TABLE 2. Geometric parameters of the coil configurations used in the validation study.

Case	Coil 1 radii $(R_{1,\text{in}}, R_{1,\text{out}})$	L_1	Coil 2 radii $(R_{2,\text{in}}, R_{2,\text{out}})$	L_2	H	Configuration type
1	(2, 2)	5	(2, 2)	5	15	Thin-wall
2	(15, 20)	5	(15, 20)	5	10	Moderate finite-radius
3	(15, 20)	5	(10, 17)	5	10	Mixed-radius
4	(10, 25)	5	(10, 25)	5	10	Large finite-radius

TABLE 3. Representative axial magnetic force predictions obtained using the three computational approaches.

Case	Semi-analytical method $\lvert F_z\rvert$ (N)	Filament-based method $\lvert F_z\rvert$ (N)	Numerical integration $\lvert F_z\rvert$ (N)	Mean force $\bar{F}$ (N)	Relative half-spread δ_{half} (%)
1	2.05×10^{-5}	2.05×10^{-5}	2.13×10^{-5}	2.08×10^{-5}	1.9
2	5.30×10^{-2}	4.90×10^{-2}	4.90×10^{-2}	5.03×10^{-2}	4.0
3	2.70×10^{-2}	2.50×10^{-2}	2.60×10^{-2}	2.60×10^{-2}	3.8
4	2.80×10^{-2}	2.70×10^{-2}	2.60×10^{-2}	2.70×10^{-2}	3.7

4. large finite-radius configuration, representing coils with a wider radial current distribution.

For finite-volume coils, the current density is calculated from

$$J_{\phi,i} = \frac{N_i I_i}{(R_{i,\text{out}} - R_{i,\text{in}})\, L_i}.$$

For the thin-wall case, where $R_{\text{in}} = R_{\text{out}}$, the volumetric current-density expression is not used directly because the radial thickness is zero. Instead, this case is treated as a surface-current or filament-limit configuration, consistent with the loop-based formulation.

The geometric parameters used in the validation study are summarized in Table 2. All dimensions in the table are given in centimeters and were converted to SI units before numerical evaluation. In all validation cases, unless otherwise specified, the coils were assigned identical electrical excitation values of

$$I_1 = I_2 = 1\,\text{A}, \quad N_1 = N_2 = 100\,\text{turns},$$

corresponding to 100 A-turns per coil. These values were kept constant for all three computational methods so that the comparison isolated the effects of geometry, separation distance, and numerical discretization.

The value of H in Table 2 denotes the representative separation used for the force comparison in Table 3. The force-distance behavior in Figure 1 was obtained by sweeping H over the plotted separation range.

4.2. Comparison of Force Predictions

The axial magnetic force was calculated for each validation case using the three computational methods. The comparison was performed under identical geometric and electrical conditions so that differences among the results reflect only the computational treatment of the interaction kernel and the discretization strategy.

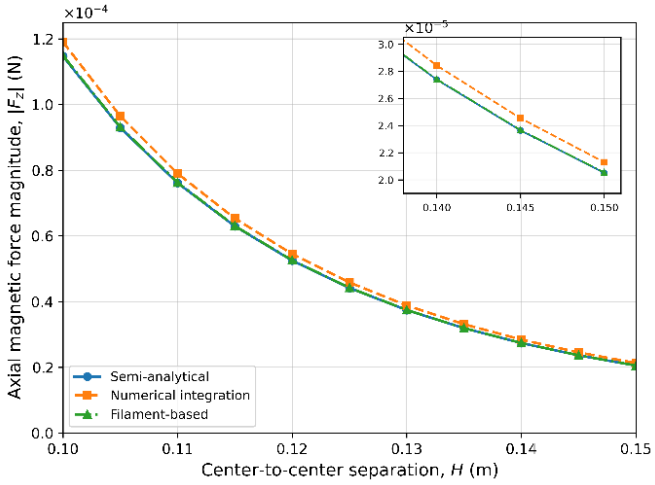

FIGURE 1. Axial magnetic force magnitude $|F_z|$ as a function of center-to-center separation distance H for the thin-wall validation case. The semi-analytical, direct numerical integration, and filament-based methods show close agreement over the investigated separation range. The inset provides a zoomed view of the small differences among the three methods near the representative validation point.

Table 3 summarizes representative force predictions for the four validation cases. The relative half-spread among the three methods is defined as

$$\delta_{\text{half}} = 100\frac{F_{\max} - F_{\min}}{2\bar{F}},$$

where

$$F_{\max} = \max\left(|F_1|, |F_2|, |F_3|\right),$$
$$F_{\min} = \min\left(|F_1|, |F_2|, |F_3|\right),$$

and

$$\bar{F} = \frac{|F_1| + |F_2| + |F_3|}{3}.$$

Here, F_1, F_2, and F_3 denote the force values obtained using the semi-analytical elliptic-integral, filament-based mutual-inductance, and direct numerical integration methods, respectively.

The results show close numerical agreement among the three methods. The smallest relative half-spread occurs for the thin-wall case because this geometry is closest to the circular-loop assumption used in the elliptic-integral and mutual-inductance formulations. The moderate finite-radius, mixed-radius, and large finite-radius cases show slightly larger differences because the current is distributed over a finite radial and axial region, making the result more sensitive to quadrature resolution and filament discretization.

Overall, the relative half-spread remains below approximately 4% for the representative cases considered. This agreement supports the internal consistency of the unified formulation and confirms that the three computational approaches produce comparable force predictions under the same idealized coaxial air-core assumptions.

4.3. Dependence of Axial Force on Separation Distance

The dependence of axial magnetic force on the center-to-center separation distance H was evaluated by varying the axial spacing between the two coils. For the representative separation sweep, the computed force magnitude decreases monotonically as H increases. This behavior is physically expected because the magnetic coupling between the two current distributions weakens as the separation distance increases.

At smaller separation distances, the magnetic interaction is stronger, and the predicted force magnitude increases. This trend is especially pronounced for configurations with concentrated current distributions or larger effective loop coupling. In contrast, finite-volume coils exhibit smoother force-distance behavior because the current density is distributed over a wider radial and axial region.

Figure 1 shows the force-distance behavior for the representative thin-wall validation case. The three computational methods reproduce the same monotonic trend and remain close to one another over the investigated separation range. Because the predicted curves nearly overlap, a zoomed inset is included to highlight the small differences among the three methods in the short-separation region.

4.4. Influence of Coil Geometry

The effect of coil geometry was investigated by comparing the force predictions for the four validation configurations listed in Table 2. The results show that coil radius, radial thickness, and geometric symmetry significantly influence the axial force magnitude.

Increasing the effective radius generally increases the magnetic interaction because the current-loop area becomes larger. Larger loop areas produce stronger magnetic coupling for a given current and separation distance. This effect is reflected in the finite-radius configurations, where the force magnitude is greater than that of the small-radius thin-wall case.

The mixed-radius case produces a different force level from the symmetric cases because the radial current distributions of the two coils do not overlap as effectively. This reduces the effective magnetic coupling between the two winding regions. The result demonstrates that the proposed framework can capture the influence of asymmetric coil geometry, provided that the coils remain perfectly coaxial.

Finite radial thickness also affects the force distribution. Compared with idealized thin-wall coils, finite-volume coils produce a spatially averaged interaction because the current density is distributed over a radial and axial cross-section. This reduces sensitivity to local geometric features and produces smoother variation of force with separation distance.

These results confirm that the proposed methods are not only limited to ideal loop geometries but can also treat finite-dimensional coaxial air-core coils within the assumptions of the model.

4.5. Discretization Sensitivity and Convergence

The numerical integration and filament-based methods require discretization of the coil geometry. Therefore, convergence tests were performed to evaluate the influence of grid refinement on the predicted force.

For the direct numerical integration method, the radial, axial, and relative azimuthal grid densities were progressively increased. The relative force error was calculated as

$$\varepsilon = \frac{|F_\Delta - F_{\text{ref}}|}{|F_{\text{ref}}|}$$

where F_Δ is the force predicted at normalized grid step size Δ, and F_{ref} is the finest-grid numerical solution.

For sufficiently smooth integrands, the composite trapezoidal rule has second-order convergence,

$$\varepsilon = O(\Delta^2),$$

where Δ is the characteristic normalized grid spacing. The numerical results follow this expected trend approximately, although the observed convergence rate may be affected by near-singular behavior when interacting current elements are close to one another.

Figure 2 shows the log-log convergence behavior of the direct numerical integration method. The relative force error decreases as the normalized grid step size is reduced. The dashed reference line represents the expected $O(\Delta^2)$ behavior of the composite trapezoidal rule. The numerical results are consistent with second-order convergence over the investigated discretization range.

For the filament-based method, convergence was assessed by increasing the number of circular filaments used to represent each coil. Increasing the filament grid from 11×11 to 21×21 changed the computed force by less than approximately 3% for the representative finite-volume cases. Further refinement produced smaller changes but increased computational cost.

TABLE 4. Main error sources in the proposed computational framework.

Error source	Affected method	Effect on force prediction	Mitigation
Quadrature error	Semi-analytical and direct numerical integration	Inaccurate evaluation of radial, axial, or angular integrals	Refine grid resolution and use convergence testing
Filament discretization error	Filament-based method	Approximation of continuous current distribution by finite loops	Increase radial and axial filament density
Near-singular kernel behavior	Direct numerical and filament-based methods	Larger error when current elements are very close	Use finer grids near small separations and avoid overlapping current volumes
Elliptic-integral evaluation near $k \to 1$	Semi-analytical and filament-based methods	Possible numerical sensitivity for closely spaced loops	Use stable elliptic-integral routines and limiting-case handling
Geometric idealization	All methods	Difference from practical wound coils	Clearly state assumptions and compare with experiments in future work
Current-density approximation	All methods	Neglect of winding pitch, discrete turns, and local axial current components	Treat the model as a continuous-current approximation

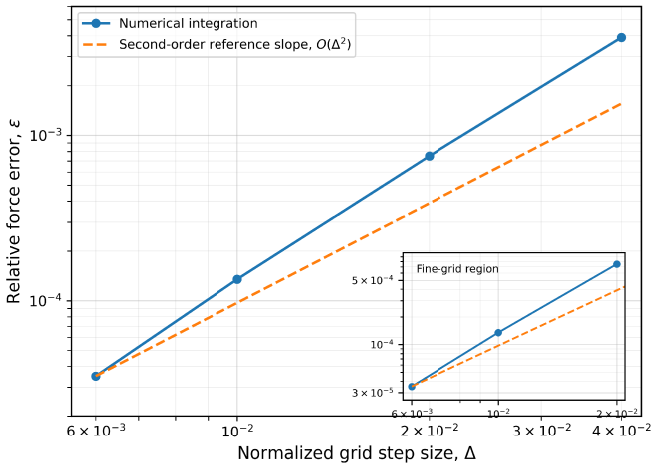

FIGURE 2. Log-log convergence behavior of the direct numerical integration method. The relative force error $\varepsilon = |F_\Delta - F_{\text{ref}}|/|F_{\text{ref}}|$ is plotted as a function of the normalized grid step size Δ, where F_{ref} is the finest-grid numerical solution. The dashed line represents an $O(\Delta^2)$ reference slope corresponding to the expected second-order behavior of the composite trapezoidal rule. The numerical results show decreasing error with grid refinement and are consistent with second-order convergence. The inset highlights the fine-grid region.

4.6. Error Sources and Uncertainty Analysis

The differences among the three computational methods arise from several numerical and modeling sources. Table 4 summarizes the main error sources considered in this study.

The most important numerical errors are quadrature error and filament discretization error. Quadrature error decreases with grid refinement in the direct numerical integration method, while filament discretization error decreases as the number of circular current loops is increased.

The most important modeling errors arise from the assumptions of air-core material, perfect coaxial alignment, uniform purely azimuthal current density, and steady current excitation. These assumptions make the formulation transparent and computationally efficient, but they also limit direct application to systems with magnetic cores, misalignment, nonlinear materials, transient excitation, or strongly discrete winding effects.

4.7. Computational Performance

The computational cost of the three methods was compared using the same validation geometries and the same implementation environment. Table 5 summarizes representative runtime values.

The semi-analytical elliptic-integral method has the lowest computational cost because the angular interaction is evaluated through elliptic-integral expressions. It is therefore suitable for rapid parameter sweeps and preliminary design studies.

The direct numerical integration method is the most computationally expensive because it evaluates the multidimensional Lorentz-force integral directly. However, it provides a useful reference calculation because it preserves the original structure of the governing force formulation.

The filament-based method provides an intermediate approach. It is faster than direct numerical integration and more flexible than a single analytical loop expression because finite coil volumes can be represented by a structured array of circular filaments.

The runtime comparison should be interpreted only for the idealized coaxial air-core configurations considered in this study. The present methods are not intended to replace general-purpose finite-element analysis for systems involving magnetic materials, nonlinear permeability, complex geometry, or misalignment.

4.8. Validation Interpretation

The validation results demonstrate that the three methods give mutually consistent axial-force predictions for the representative coaxial air-core coil geometries considered. This agreement is meaningful because the methods evaluate the force using different computational routes: elliptic-integral reduction, direct Lorentz-force integration, and filament-based mutual-inductance summation.

TABLE 5. Representative computational performance of the proposed methods.

Method	Representative agreement level	Average runtime (s)	Main use
Semi-analytical elliptic-integral method	Relative half-spread below approximately 4% in the validation cases	0.2	Rapid parametric evaluation and benchmark calculation
Direct numerical integration method	Reference numerical calculation	11.5	Direct evaluation of the Lorentz-force integral
Filament-based mutual-inductance method	Relative half-spread below approximately 4% in the validation cases	1.2	Engineering-scale estimation and preliminary design

However, the comparison should be interpreted as computational cross-validation rather than experimental validation. Since all three methods are derived from the same physical assumptions, agreement among them confirms internal consistency but does not quantify deviations caused by real winding geometry, manufacturing tolerances, material effects, current distribution nonuniformity, or measurement uncertainty.

Therefore, the present validation supports the correctness and numerical stability of the proposed formulation within its stated assumptions. Future experimental measurements or independent finite-element benchmarks would be required to evaluate the model's accuracy for practical coil assemblies.

4.9. Summary of Results

The results of the validation study can be summarized as follows. The three computational methods produce consistent axial-force predictions for thin-wall, moderate finite-radius, mixed-radius, and large finite-radius coaxial air-core coil configurations. The axial force decreases monotonically with increasing center-to-center separation, consistent with the expected reduction in magnetic coupling.

The relative half-spread among the three methods remains below approximately 4% for the representative cases considered. The direct numerical integration and filament-based methods exhibit stable convergence with grid refinement. The semi-analytical method is the fastest approach and is suitable for rapid parametric studies, while the direct numerical integration method provides the most direct reference implementation of the Lorentz-force formulation. The filament-based method offers a practical balance between speed and flexibility.

Overall, the results support the proposed unified framework as a reliable computational benchmark for axial magnetic force evaluation in idealized perfectly coaxial air-core coil systems.

5. DISCUSSION

The results presented in Section 4 demonstrate that the three computational approaches developed in this work provide mutually consistent predictions of the axial magnetic force between perfectly coaxial air-core cylindrical coils over the representative geometries considered. Since the semi-analytical elliptic-integral method, the direct numerical integration method, and the filament-based mutual-inductance method are all derived from the same Biot-Savart and Lorentz-force formulation, their agreement supports the internal consistency of the proposed unified framework.

However, this agreement should be interpreted carefully. The comparison among the three methods provides computational cross-validation, not experimental validation. Because all three approaches share the same physical assumptions, agreement among them confirms that the mathematical formulation and numerical implementations are consistent within the idealized model. It does not, by itself, quantify deviations that may arise in practical wound coils due to manufacturing tolerances, helical winding pitch, conductor spacing, misalignment, magnetic materials, or measurement uncertainty.

A key outcome of this study is that the three methods exhibit complementary strengths. The semi-analytical elliptic-integral method provides the highest computational efficiency and is suitable for rapid parametric studies and benchmark calculations. The direct numerical integration method preserves the original Lorentz-force interaction structure and provides a transparent numerical reference. The filament-based mutual-inductance method offers a practical compromise between computational cost and modeling flexibility by representing the finite coil volume as an array of circular current filaments.

From an engineering perspective, this complementary structure is useful because different design stages require different balances among speed, transparency, and accuracy. In early-stage design, the semi-analytical and filament-based methods can be used to explore geometric trends and estimate force levels quickly. When a more direct numerical reference is needed within the assumptions of the present model, the direct numerical integration method provides a useful comparison tool.

5.1. Practical Relevance and Potential Applications

Although the present study is intentionally restricted to idealized coaxial air-core coils, the proposed framework is relevant to several engineering and scientific applications in which axial magnetic interaction is important. These include electromagnetic actuators, inductive coupling systems, wireless power transfer devices, precision force-calibration devices, laboratory coil test platforms, and preliminary design studies for electromechanical systems.

In electromagnetic actuators, the axial force between coils directly affects stroke control, force density, and mechanical response. In inductive coupling and alignment-sensitive devices, axial force variation with separation can influence sta-

TABLE 6. Main assumptions of the proposed framework and their practical implications.

Assumption	Role in the formulation	Practical implication
Air-core medium, $\mu_r = 1$	Allows use of the free-space Biot-Savart formulation	Magnetic cores, saturation, hysteresis, and nonlinear permeability are not included
Perfect coaxial alignment	Ensures cylindrical symmetry and cancellation of transverse force components	Lateral offset or angular tilt can generate radial and tangential forces not captured here
Uniform purely azimuthal current density	Simplifies the coil current distribution to $\mathbf{J} = J_\phi \hat{\boldsymbol{\phi}}$	Axial current components, winding pitch, end effects, and local conductor routing are neglected
Steady current excitation	Enables magnetostatic treatment	Eddy currents, time-varying fields, and transient effects are not modeled
Continuous winding approximation	Replaces discrete turns by an equivalent current density	Turn spacing, insulation, conductor shape, and local current nonuniformity are not explicitly represented

bility and positioning behavior. In calibration systems and laboratory platforms, transparent benchmark models are useful for verifying numerical solvers and comparing computational approaches.

The proposed framework is particularly useful when the system geometry is close to the idealized assumptions considered in this work: air-core coils, steady currents, perfect coaxial alignment, and uniform azimuthal current density. Under these conditions, the methods provide fast and physically interpretable force estimates without requiring repeated full finite-element simulations.

However, for systems involving magnetic cores, nonlinear materials, complex conductor routing, significant misalignment, or transient excitation, the present model should be regarded as a benchmark or preliminary design tool rather than a complete replacement for full-field electromagnetic simulation.

5.2. Interpretation of the Unified Framework

The main contribution of this work is the unification of three commonly used modeling routes within one consistent derivational structure. The study does not propose a new electromagnetic law. Instead, it shows how the axial magnetic force between finite coaxial air-core coils can be evaluated using three related but computationally different methods derived from the same physical foundation.

This unified treatment addresses a practical gap in coil-force modeling. Analytical elliptic-integral methods are often efficient but specialized. Direct numerical integration is general within the assumed geometry but computationally more expensive. Filament-based methods are intuitive and flexible but require discretization choices. Presenting these approaches together allows their assumptions, accuracy, convergence behavior, and computational cost to be compared under identical coil geometries and current distributions.

This is useful for two reasons. First, it provides a transparent benchmark structure for researchers and engineers who need reliable reference calculations for coaxial air-core coils. Second, it helps identify which method is most appropriate for a given modeling task. For rapid parameter sweeps, the semi-analytical method is preferable. For direct verification of the Lorentz-force formulation, the numerical integration method is more suitable. For engineering-scale approximation with moderate computational cost, the filament-based method is attractive.

5.3. Applicability and Assumptions

The validity of the proposed framework depends on the assumptions used in the derivation. These assumptions simplify the physical problem and make the formulation analytically and numerically tractable, but they also restrict the range of practical systems to which the model can be directly applied.

The most important assumptions are summarized in Table 6.

The assumption of purely azimuthal current density is especially important. In practical helical windings, a small axial current component may exist because the conductor advances along the coil axis as it is wound. The present model neglects this component and assumes

$$J_r = 0, \quad J_z = 0, \quad J_\phi \neq 0.$$

This approximation is appropriate when the coil is tightly wound, and the dominant current direction is circumferential. However, for coils with large winding pitch, complex conductor paths, or significant end connections, additional modeling would be required.

Similarly, the cancellation of radial and azimuthal force components depends on perfect cylindrical symmetry. If the coils are laterally displaced, tilted, or geometrically eccentric, the transverse components no longer vanish. Recent studies on misaligned coil pairs show that misalignment can introduce lateral-force components and significantly affect magnetic-force behavior [20]. Therefore, the present formulation should not be applied directly to misaligned systems without extension to a more general three-dimensional force model.

5.4. Error Sources and Uncertainty

The relative half-spread values reported in the validation cases arise from both numerical and modeling sources. The main numerical error sources are quadrature error, filament discretization error, near-singular kernel behavior, and numerical sensi-

tivity in elliptic-integral evaluation. The main modeling error sources are the continuous-current approximation, the neglect of axial current components, and the idealized assumptions of air-core material and perfect coaxial alignment.

In the direct numerical integration method, the dominant error source is quadrature error. The method evaluates a multi-dimensional Lorentz-force integral using discrete radial, axial, and angular grids. As the grid is refined, this error decreases, and the observed convergence behavior is consistent with the expected second-order trend of the composite trapezoidal rule for sufficiently smooth integrands. However, convergence can be slower when the interaction kernel becomes sharply varying, especially at small separations.

In the filament-based method, the main error source is the approximation of a continuous current distribution by a finite number of circular current filaments. Increasing the number of filaments improves accuracy, but also increases computational cost. The results show that practical filament densities can provide force estimates within a few percent of the comparison values for the representative geometries considered.

In the semi-analytical elliptic-integral method, numerical error is generally small because the angular dependence is handled analytically. Nevertheless, care is required when the elliptic modulus approaches unity, which may occur for closely spaced loop elements. Stable numerical routines and limiting-case handling are important in such cases.

The modeling uncertainty is more difficult to quantify because it depends on how closely a real coil matches the idealized assumptions. Practical factors such as winding pitch, finite conductor diameter, turn spacing, insulation, coil support structures, and current distribution nonuniformity can introduce deviations from the continuous-current model. Therefore, the relative half-spread values below approximately 4% reported among the three methods should be understood as agreement within the idealized computational model, not as a universal accuracy bound for all physical coil systems.

5.5. Validation Scope

The validation presented in this study consists of analytical and numerical cross-comparison among three independently implemented computational routes. This is valuable because the methods evaluate the same physical quantity in different ways: elliptic-integral reduction, direct Lorentz-force integration, and mutual-inductance-based filament summation.

The close agreement among the methods indicates that the derived expressions are numerically consistent and that the implementations are stable for the validation geometries considered. The monotonic decrease of force with increasing separation distance also agrees with the expected physical behavior of coaxial current-carrying coils.

Nevertheless, the present validation does not replace experimental verification. Experimental validation would require measuring the force between physical coil pairs under controlled current, geometry, and separation conditions. Such measurements would allow the model error associated with winding pitch, conductor geometry, mechanical tolerances, and measurement uncertainty to be quantified.

Therefore, the present results should be interpreted as demonstrating computational reliability and internal consistency for the idealized model. Future experimental work would be needed to establish quantitative accuracy for practical manufactured coil systems.

5.6. Comparison with Finite-Element Modeling

Finite-element modeling remains a more general approach for electromagnetic systems involving complex geometry, nonlinear magnetic materials, magnetic cores, shielding, eddy currents, or misalignment. The proposed methods are not intended to replace finite-element analysis in such cases.

The advantage of the present framework is its efficiency and transparency for the specific class of perfectly coaxial air-core coils. In this restricted setting, the semi-analytical and filament-based methods can provide rapid force estimates suitable for parameter sweeps, design-space exploration, and benchmark generation. The direct numerical integration method provides a useful reference calculation while retaining the physical structure of the Lorentz-force formulation.

Thus, the proposed framework is best viewed as complementary to finite-element modeling. It can be used to generate reference solutions, check numerical simulations, guide preliminary design, and identify trends before more detailed full-field modeling is performed.

5.7. Future Work

Several extensions would strengthen the applicability of the proposed framework.

First, experimental validation should be performed using representative air-core coil pairs. Force-distance measurements under controlled current and alignment conditions would allow direct assessment of the difference between the idealized model and real wound coils.

Second, the formulation could be extended to account for non-coaxial configurations, including lateral offset and angular misalignment. This would allow the calculation of radial and tangential force components in addition to the axial force. Such an extension would be especially important because misalignment can significantly influence force behavior in practical coil systems [20].

Third, practical winding effects could be incorporated by modeling discrete turns, helical winding pitch, finite conductor diameter, insulation spacing, and nonuniform current distributions. Such extensions would help bridge the gap between the continuous-current approximation and real coil construction.

Fourth, coupling with finite-element or reduced-order magnetic-material models could extend the method to systems involving ferromagnetic cores, magnetic shielding, or nearby conductive structures.

Finally, machine-learning-assisted surrogate models could be trained using the analytical and numerical results generated by the present framework. Such surrogate models may be useful for rapid optimization and repeated design evaluation, provided that their training data remain within the same physical assumptions and geometric domain [17, 18, 21].

5.8. Summary of Discussion

The proposed unified framework provides an efficient and physically transparent approach for evaluating axial magnetic force in idealized coaxial air-core coil systems. The three computational methods show consistent results because they are derived from the same governing electromagnetic formulation, but their agreement should be interpreted as computational cross-validation rather than experimental validation.

The framework is most useful for benchmark generation, preliminary design, numerical verification, parametric force analysis, and educational analysis of coaxial air-core coil interactions. Its limitations are directly associated with the assumptions of air-core material, perfect coaxial alignment, steady current excitation, and uniform purely azimuthal current density. Within these assumptions, the method provides a reliable and computationally efficient basis for axial force evaluation.

6. CONCLUSION

This paper has presented a unified analytical and numerical framework for evaluating the axial magnetic force between two finite-dimensional, perfectly coaxial, air-core cylindrical coils under steady current excitation. The formulation was developed from the Biot-Savart law and the Lorentz force law and was reduced using cylindrical symmetry. The model assumes a continuous, uniform, purely azimuthal current density in each coil and neglects radial and axial current components, winding-pitch effects, magnetic materials, coil misalignment, and transient electromagnetic phenomena.

From the common theoretical formulation, three computational approaches were developed and compared: a semi-analytical elliptic-integral method, a direct multidimensional trapezoidal numerical-integration method, and a filament-based mutual-inductance method. The required elliptic-integral expressions, the mutual-inductance function M, and the loop-loop force kernel were explicitly defined to provide a reproducible connection between the analytical and numerical formulations.

The methods were applied to representative coaxial coil geometries, including thin-wall, moderate finite-radius, mixed-radius, and large finite-radius configurations. The results showed consistent axial-force predictions among the three approaches, with relative half-spread values below approximately 4% for the validation cases considered. The force magnitude decreased monotonically with increasing axial separation, consistent with the expected reduction in the magnetic coupling between the coils.

The semi-analytical method provided the fastest evaluation and is suitable for rapid parametric studies and benchmark calculations. The direct numerical integration method preserved the full Lorentz-force interaction structure and served as a transparent numerical reference. The filament-based method offered a practical compromise between computational efficiency and modeling flexibility by representing finite winding regions as arrays of circular current filaments.

The validation presented in this work should be interpreted as computational cross-validation within the stated assumptions, not as experimental validation. Agreement among the three methods confirms the internal consistency of the formulation and implementation, but it does not quantify deviations associated with real winding geometry, manufacturing tolerances, conductor spacing, magnetic materials, misalignment, or measurement uncertainty.

Overall, the proposed framework provides a transparent and efficient benchmark structure for axial magnetic force evaluation in idealized coaxial air-core coil systems. It is useful for preliminary electromagnetic actuator design, numerical solver verification, parametric force analysis, and educational treatment of coil-coil magnetic interaction problems.

Future work should include experimental force-distance measurements, extension to non-coaxial and misaligned coil configurations, incorporation of discrete winding pitch and finite conductor geometry, and coupling with finite-element or reduced-order models for systems involving magnetic materials and more complex geometries.

ACKNOWLEDGEMENT

The authors gratefully acknowledge the support of the Robotic Century Innovation Laboratory for providing computational resources and technical discussions that contributed to this research.

REFERENCES

[1] Grover, F. W., *Inductance Calculations: Working Formulas and Tables*, Dover Publications, New York, NY, USA, 2004.

[2] Babic, S. I. and C. Akyel, "Calculating mutual inductance between circular coils with inclined axes in air," *IEEE Transactions on Magnetics*, Vol. 44, No. 7, 1743–1750, 2008.

[3] Rosa, E. B., "The self and mutual inductances of linear conductors," *Bulletin of the Bureau of Standards*, Vol. 4, 301–344, 1908.

[4] Kirsch, A. and F. Hettlich, *The Mathematical Theory of Time-harmonic Maxwell's Equations: Expansion, Integral, and Variational Methods*, Springer, 2016.

[5] Sondhi, K., N. Garraud, D. Alabi, D. P. Arnold, A. Garraud, S. G. R. Avuthu, Z. H. Fan, and T. Nishida, "Flexible screen-printed coils for wireless power transfer using low-frequency magnetic fields," *Journal of Micromechanics and Microengineering*, Vol. 29, No. 8, 084006, 2019.

[6] Xu, X., Z. Huang, W. Li, F. Dong, L. Hao, B. Shen, and Z. Jin, "Study on reducing the maximum perpendicular magnetic field of HTS coils used on synchronous generator armatures," *IEEE Transactions on Applied Superconductivity*, Vol. 29, No. 5, 1–5, 2019.

[7] Pankrac, V., "The algorithm for calculation of the self and mutual inductance of thin-walled air coils of general shape with parallel axes," *IEEE Transactions on Magnetics*, Vol. 48, No. 5, 1875–1889, 2012.

[8] Lemarquand, G., V. Lemarquand, S. Babic, and C. Akyel, "Magnetic field created by thin wall solenoids and axially magnetized cylindrical permanent magnets," in *PIERS Proceedings*, 614–618, Moscow, Russia, Aug. 2009.

[9] Braneshi, M., O. Zavalani, and A. Pijetri, "Evaluation of axial force between two coaxial disk coils," in *Proceedings of the 3rd International PhD Seminar on Computational Electromagnetics*, Ghent, Belgium, 2006.

[10] Ravaud, R., G. Lemarquand, S. Babic, V. Lemarquand, and C. Akyel, "Cylindrical magnets and coils: Fields, forces, and inductances," *IEEE Transactions on Magnetics*, Vol. 46, No. 9, 3585–3590, 2010.

[11] Maxwell, J. C., *A Treatise on Electricity and Magnetism*, Clarendon Press, 1873.

[12] Abramowitz, M. and I. A. Stegun, *Handbook of Mathematical Functions*, Dover Publications, New York, NY, USA, 1965.

[13] Conway, J. T., "Exact solutions for the mutual inductance of circular coils and elliptic coils," *IEEE Transactions on Magnetics*, Vol. 48, No. 1, 81–94, 2012.

[14] Palka, R., "Fast analytic-numerical algorithms for calculating mutual and self-inductances of air coils," *Energies*, Vol. 17, No. 2, 325, 2024.

[15] Babic, S., E. Guven, K.-H. Song, and Y. Luo, "Optimized calculation of radial and axial magnetic forces between two non-coaxial coils of rectangular cross-section with parallel axes," *Computation*, Vol. 12, No. 9, Art. no. 180, 2024.

[16] Wang, Y., X. Xie, and H. Wang, "Spatial magnetic field calculations for coreless circular coils with rectangular cross-section of arbitrary turn numbers," *Progress In Electromagnetics Research M*, Vol. 101, 9–23, 2021.

[17] Giovannetti, G., N. Fontana, A. Flori, M. F. Santarelli, M. Tucci, V. Positano, S. Barmada, and F. Frijia, "Machine learning for the design and the simulation of radiofrequency magnetic resonance coils: Literature review, challenges, and perspectives," *Sensors*, Vol. 24, No. 6, Art. no. 1954, 2024.

[18] Barmada, S., N. Fontana, L. Sani, D. Thomopulos, and M. Tucci, "Deep learning and reduced models for fast optimization in electromagnetics," *IEEE Transactions on Magnetics*, Vol. 56, No. 3, Art. no. 7513604, 2020.

[19] Landreman, M., S. Hurwitz, and T. M. Antonsen, "Efficient calculation of self magnetic field, self-force, and self-inductance for electromagnetic coils with rectangular cross-section," *Nuclear Fusion*, Vol. 65, No. 3, 036008, 2025.

[20] Yang, Y., W. S. P. Robertson, A. Jafari, and M. Arjomandi, "Optimising coil design based on sensitivity analysis of magnetic force induced between misaligned coil pairs," *Electrical Engineering*, Vol. 107, 15 317–15 328, 2025.

[21] Khan, A., V. Ghorbanian, and D. Lowther, "Deep learning for magnetic field estimation," *IEEE Transactions on Magnetics*, Vol. 55, No. 6, Art. no. 7202304, 2019.